Disorder-Induced Phase Transitions in the Transmission of Dielectric Metasurfaces

A. Rahimzadegan,[1,*] D. Arslan,[2,†] R. N. S. Suryadharma,[1] S. Fasold,[2] M. Falkner,[2]
T. Pertsch,[2] I. Staude,[2] and C. Rockstuhl[1,3]

[1]*Institute of Theoretical Solid State Physics, Karlsruhe Institute of Technology, 76131 Karlsruhe, Germany*
[2]*Institute of Applied Physics, Abbe Center of Photonics, Friedrich Schiller University Jena, 07745 Jena, Germany*
[3]*Institute of Nanotechnology, Karlsruhe Institute of Technology, 76021 Karlsruhe, Germany*

(Received 3 September 2018; revised manuscript received 19 November 2018; published 9 January 2019)

Light interaction with disordered materials is both complex and fascinating at the same time. Here, we reveal disorder-induced phase transitions in a dielectric Huygens' metasurface made from silicon nanocylinders that simultaneously support an electric and magnetic dipole resonance. Depending on the degree of positional disorder and the spectral detuning of the two resonances, the phase angle of the transmission coefficient exhibits a clear phase transition from normal to anomalous dispersion. Combined with the considerations of whether the resonances of spectrally detuned particles appear as separated or overlapping, we distinguish four different phase states. We study this phenomenon analytically by employing dipole particles and disclose the entire phase diagram, support our insights with full-wave simulations of actual structures, and corroborate the findings with experimental results. Unveiling this phenomenon is a milestone simultaneously in the growing fields of metamaterial-inspired silicon nanophotonics, photonics in disordered media, and the fundamental physics of phase transitions.

DOI: 10.1103/PhysRevLett.122.015702

Huygens' metasurfaces made from dielectric high-permittivity nanocylinders offer suppressed reflection and a near-unity transmittance over a wide spectral range [1–3]. Ideally, the induced electric and magnetic dipole moments in any of the nanocylinders should be identical. When combined with the discrete rotational symmetry [$R_z(2\pi/n)$ for $n \geq 3$] of their arrangement [4], reflection is suppressed for all incident polarizations and the phase angle of the transmission coefficient can be adjusted on demand [5]. Indeed, the entire phase angle range of 2π is accessible within the spectral range of the resonances. Hence, Huygens' metasurfaces are a cornerstone for future photonic architectures that aim to steer light on demand with highest efficiency [6–8].

In general, the phase angle of the transmission coefficient possesses normal dispersion; i.e., the accumulated phase angle decreases as the wavelength increases [9]. However, the near-resonance optical response of metasurfaces is very sensitive to the spacing among neighboring nanocylinders, and a quite far-reaching interparticle interaction is observed [10]. This sensitivity triggers the question concerning the influence of positional disorder on the spectral characteristics of such metasurfaces.

Disorder itself unlocks a plethora of physical effects worth exploring, not only out of intellectual curiosity but also from an application perspective [11–18]. Here, we study the impact of positional disorder in the arrangement of the nanocylinders on the optical response of a Huygens' metasurfaces and reveal intriguing phase transitions in the phase angle of the metasurface's transmission.

Phase transitions are ubiquitous phenomena. The fascination for their exploration is derived from the fact that an incremental change to a given system in one of the control parameters does not just give rise to an incremental change in the emerging properties of the system but, quite in contrast, gives rise to a qualitatively different behavior at particular points of operation. There are plenty of examples in solid state physics, where phase transitions in material properties have been described depending on, e.g., a critical pressure or a critical temperature [19,20]. Multiple photonic devices derive their functionalities from such phase transitions in the material properties [21–23]. Phase transitions have also been studied in the field of photonics. Prime examples concern the change from an elliptical to a hyperbolic dispersion relation for certain strongly anisotropic metamaterials at a critical wavelength [24,25], the change from a metamaterial to a photonic crystal [26], the change from a real to a complex valued spectrum at the spontaneous breakdown of the $\mathcal{PT}$ symmetry of a given optical potential [27,28], or the change from a topological trivial to a topological nontrivial band structure of a photonic material upon suitable geometrical deformations [29].

The largest share of attention in the field of photonics has possibly been drawn to disorder-induced phase transitions, where they have been decisive in the exploration of photonic band gaps [30]. Light is then said to be localized above a critical threshold for the disorder depending on the dimensionality [31–34]. With that, disorder was shown to be not just a nuisance [35,36], but it constitutes a valuable

resource on which we can capitalize to tailor the propagation of light [37–39].

In this contribution, we reveal and explore disorder-induced phase transitions in the phase angle of the transmission coefficient of a Huygens' metasurface, which are likely to find application in novel phase-manipulating optical devices. More technical information on all the steps can be found in the Supplemental Material (SM) [40].

Our aim here is not to define a new universal disorder metric, which might even be a vain endeavor [41–48], but rather to study the effect of disorder on the optical properties of metasurfaces in transmission. Note that the wavelength-dependent transmission coefficient itself already serves as a global posterior measure of disorder.

Analytical model.—In order to reveal the basic mechanisms of this effect, we rely on an analytical approach in which the electric and magnetic dipole polarizabilities of all particles forming the metasurface are considered to be identical and to possess a Lorentzian line shape [49–53]. Higher order multipole moments are not considered. Particles with such identical electric and magnetic polarizabilities are said to have electromagnetic duality symmetry [54,55], and hence are called dual particles. The dual particles defined in our analysis are isotropic and non-absorbing point dipoles with a resonance wavelength of $\lambda = 1\ \mu$m. The corresponding polarizabilities of these particles were assumed to have a full width at half maximum of 50 nm (see SM, Sec. I A).

The starting point of our analysis is a square array of dual particles, which we refer to as a dual metasurface, with a lattice constant of $a = 800$ nm, and we consider transmission through this metasurface. In the following, we systematically perturb the particle positions, and hence refer to the square array as the configuration with vanishing positional disorder. As the simulation of an infinite array with positional disorder is not feasible, we restrict our analysis to an array of $17 \times 17 = 289$ dual particles. The metasurfaces are illuminated in the simulation by a fundamental transverse Gaussian beam with a waist diameter that is smaller than the spatial extent of the finite structure. The wavelength-dependent complex-valued transmission coefficient in forward direction $t(\lambda)$ is calculated using an analytical local coordinate T-matrix method [56,57] (see SM, Sec. I B).

The analytical results for the transmission through a metasurface with vanishing positional disorder are shown in Figs. 1(a) and 1(b) with a dotted line and cross markers. Figure 1(a) shows a parametric plot of $t(\lambda)$ as a function of its real and imaginary part and the wavelength as the parameter. The wavelengths are encoded by rainbow colors and correspond to those used in the abscissa of Fig. 1(b). Figure 1(b) shows the phase angle $\phi_t(\lambda)$ of $t(\lambda)$ as a function of the wavelength. As the wavelength increases, the amplitude $|t(\lambda)|$ stays near unity and $\phi_t(\lambda)$ varies over almost 2π with normal dispersion. In Fig. 1(a), this behavior can be seen as an almost fully circular path that circles the origin of the complex plane clockwise.

Disordered metasurfaces.—To study the effect of positional disorder on the transmission coefficient of dual metasurfaces, we gradually perturb the particle positions in the square array and calculate $t(\lambda)$. We call these arrangements as perturbed square array. In particular, centered at each lattice site, we define a square area with side lengths of $\Delta r = \mathcal{PD} \times a$ and a uniform probability density function from which we draw the perturbed particle coordinate. The aforementioned equation implicitly defines the positional disorder as $\mathcal{PD} \in [0, 1]$. In Figs. 1(a)–1(d), we visualized $t(\lambda)$ for 0%, 30%, 60%, and 80% of positional disorder. There are two interesting findings not yet discussed in the literature:

(i) *Insensitivity to positional disorder.*—From Fig. 1(b) it is seen that with increasing positional disorder, prior to reaching a critical threshold, $\phi_t(\lambda)$ remains almost completely unaltered, which suggests that the phase angle is very resistant to positional disorder. This is a very important finding that might find applications in phase-manipulating optical devices.

(ii) *Disorder-induced phase transition.*—In Fig. 1(b), spectral regions with anomalous dispersion are observed when the positional disorder exceeds a critical threshold. Indeed, the advance of $\phi_t(\lambda)$ above this critical threshold is increasing with increasing wavelength. The underlying physics can be revealed by inspecting the dispersive behavior of $t(\lambda)$ in the complex plane, as shown in Fig. 1(a). As the positional disorder is increased, the path traced out by $t(\lambda)$ contracts towards a point well within the positive real half-space. For low positional disorder, the path circles the origin of the complex plane clockwise. For high positional disorder, the path does not circle the origin anymore, i.e., at a vanishing imaginary part of $t(\lambda)$, the real part is always positive. We take this from now on as one objective criteria to classify our phase state. We distinguish between phase states in where the phase angle shows normal and anomalous dispersion, respectively. At the critical threshold, $|t(\lambda)|$ undergoes a root; i.e., the path passes exactly through the origin, and $\phi_t(\lambda)$ abruptly changes from normal to anomalous dispersion. At this point of operation, the metasurface radiates all the light in nonspecular directions; i.e., the light is neither transmitted in a forward direction nor reflected in a backward direction. Similar to critical coupling in perfect absorbers [58], at this phase transition, the effective electric and magnetic dipole moments are halved in strength and hence the forward and backward scattering is diminished. However, unlike the perfect absorbers, where the absorption losses are the prime cause of this reduction, here, the radiation losses due to the positional disorder are the prime reason. A further increase in the positional disorder only further contracts the path and $\phi_t(\lambda)$ continues to exhibit anomalous dispersion. With that we observe a

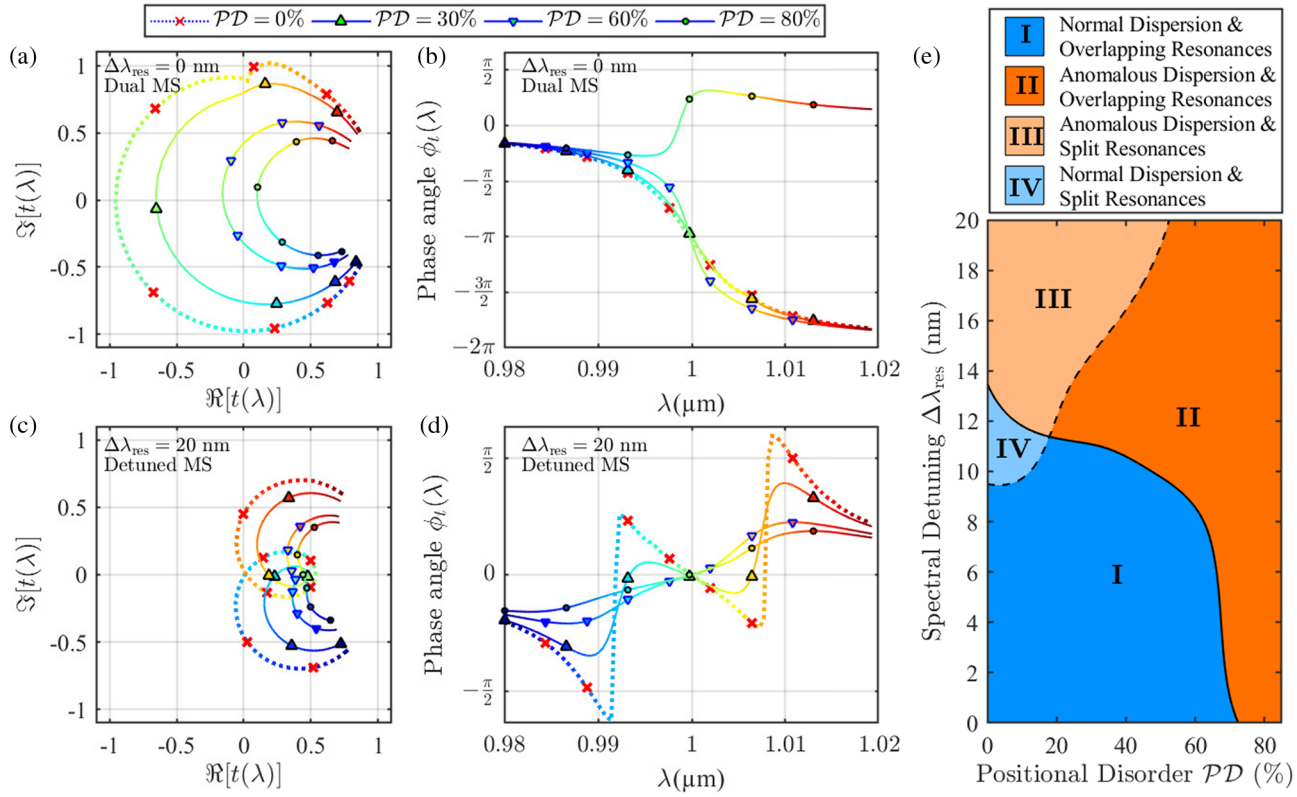

FIG. 1. The effect of positional disorder on dual and detuned metasurfaces with a perturbed square array arrangement. Transmission coefficient $t(\lambda)$ of (a),(b) dual and (c),(d) detuned metasurfaces. (b),(d) Spectra of the phase angle $\phi_t(\lambda)$ of $t(\lambda)$ and (a),(c) parametric plots of the respective $t(\lambda)$ in dependence on the wavelength. Each metasurface consists of nonabsorbing point-dipole particles that have a Lorentzian line shape with a full width at half maximum of 50 nm, and a spectral detuning of $\Delta\lambda_{res}$ among their electric and magnetic polarizability resonances. The reference metasurface ($\mathcal{PD} = 0\%$) is a square array with lattice constant $a = 800$ nm. The wavelengths are encoded by rainbow colors and correspond to those used on the abscissa of (b),(d). The line markers encode the degree of positional disorder. (e) Phase diagram as a function of positional disorder $\mathcal{PD}$ and spectral detuning $\Delta\lambda_{res}$.

sharp transition from normal to anomalous dispersion at a critical threshold for the positional disorder.

Disordered and detuned metasurfaces.—Next, we study the impact of positional disorder on spectrally detuned metasurfaces. By spectrally detuned metasurface we refer to a metasurface for which the electric and magnetic dipole resonances of its particles, which up to now had been at identical spectral position, are spectrally shifted apart from each other by $\Delta\lambda_{res}$. Our analytical approach allows us to systematically increase the spectral detuning $\Delta\lambda_{res}$ for the previously considered dual particles. We consider here a range from 0 nm up to 20 nm.

For large spectral detuning of 20 nm and vanishing positional disorder, the two resonances are clearly distinguishable from each other in the $\phi_t(\lambda)$ spectrum, as can be seen in Fig. 1(d). In Fig. 1(c), the two resonances manifest in the complex plane as a crunode, which is a point where the path of $t(\lambda)$ is intersecting itself and thereby forming a loop. As the positional disorder is increased from 0% to 85%, the path contracts again and the crunode vanishes at a critical threshold for the positional disorder. Above this critical threshold, the two resonances cannot be distinguished from each other anymore and appear instead as a single resonance. Hence, for large spectral detuning we observe a sharp transition from a state with spectrally split resonances to a state with spectrally overlapping resonances at a critical threshold for the positional disorder. Additionally, we notice that, according to the just introduced definitions, we always observe spectral regions of anomalous phase angle advance independent of the positional disorder for the detuned metasurface.

In summary, we observed disorder-induced phase transitions in two distinct properties of the $\phi_t(\lambda)$ spectrum: On the one hand, the dispersion switches from a state with *normal dispersion* (ND) to a state with *anomalous dispersion* (AD), and on the other hand, the apparent number of resonances switches between a state with *split resonances* (SR) to a state with *overlapping resonances* (OR). In the complex plane, we distinguish between ND and AD whether the path of $t(\lambda)$ circles the origin or not, and between SR and OR whether the path possesses a crunode or not, respectively. Consequently, four distinct phase states can be identified: Phase state *I* (ND and OR),

phase state *II* (AD and OR), phase state *III* (AD and SR), and phase state *IV* (ND and SR).

The phase diagram in Fig. 1(e) visualizes our findings that were obtained from a systematic analysis of wide ranges of positional disorder $\mathcal{PD} = 0, 5, \ldots, 85\%$ and spectral detuning $\Delta\lambda_{\mathrm{res}} = 0, 1, \ldots, 20$ nm. The phase state boundaries are smoothed for easier interpretation (see SM, Sec. II C).

At the quadruple point of the phase diagram, the path of $t(\lambda)$ passes exactly through the origin of the complex plane, which marks the transition between ND and AD, and, also, exhibits a crunode somewhere in the complex plane, which marks the transition between OR and SR.

For infinitely extended nonabsorbing square arrays with vanishing positional disorder, we do not observe phase state *IV*. In this particular case, the crunode is forming exactly in the origin of the complex plane, causing a direct transition from phase state *I* to phase state *III*. For finite arrays we observe a weak dependence of the location of the quadruple point in the phase diagram on the array size.

Experimental result and numerical verification.— To experimentally observe the different phase states of $\phi_t(\lambda)$, we fabricated metasurfaces consisting of silicon nanocylinders on a silica substrate and embedded them in a 1 μm thick silica layer (see SM Sec. VI).

The ability to alter the nanocylinders' aspect ratio and the square arrays' lattice constant allows us to control the spectral detuning of the resonances in the electric and magnetic polarizabilities [10,59]. For a given lattice constant, we optimized in an initial design process, using COMSOL Multiphysics, the aspect ratio of the silicon nanocylinders of a metasurface with vanishing positional disorder such that the transmittance is maximized within the spectral range of the resonances. We found for a lattice constant of $a = 800$ nm the optimal height ($h = 220$ nm) and radius ($r = 245$ nm) of the silicon nanocylinders.

A minimum distance of 80 nm between the silicon nanocylinders was required to avoid neighboring nanocylinders from merging to a single entity in the fabrication process. Together with the finite size of these particles, the maximum possible perturbation for our system ($\mathcal{PD}_{\mathrm{max}} \approx 30\%$) was deemed to be too small to exhibit the phase transition from phase state *I* to phase state *II*. To observe the different phase states, we hence resorted to a different particle distribution with less constraints in the positioning of the nanocylinders.

We made use of a generalized Matérn type-III point processes for the generation of point patterns, which serve as the center points of the silicon nanocylinders [60,61]. More precisely, we parametrized the Matérn model with respect to two characteristic radii α and β (see SM Sec. III), and fabricated two metasurfaces that we labeled as Matérn type-III soft-core distributions ($\alpha = 0.57$ μm, $\beta = 0.8$ μm) and Matérn type-III hard-core distributions ($\alpha = \beta = 0.57$ μm). The resulting particle distributions are highly uniform and isotropic, and their average particle density was set equal to that of a square array. Scanning electron micrographs of fabricated metasurfaces based on a square array, perturbed square array, Matérn type-III soft-core and hard-core distributions are shown in Fig. 2. Each of the metasurfaces covers a square area of 2×2 mm^2. Statistical details of these samples are discussed in the SM (see Sec. IV).

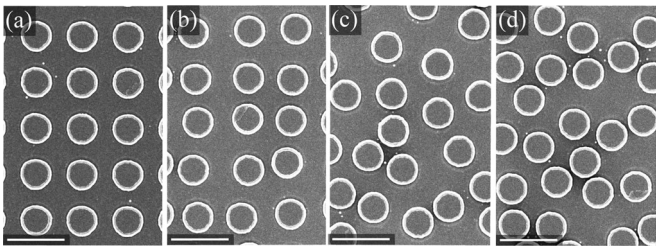

FIG. 2. Scanning electron micrographs of silicon nanocylinders before embedding in fused silica, arranged in a (a) square array, (b) perturbed square array, (c) Matérn type-III soft-core, and (d) hard-core distribution. All scale bars, 1 μm.

After fabrication, we measured the transmittance spectra $|t(\lambda)|^2$ and the phase angle spectra $\phi_t(\lambda)$ of each metasurface. We used an interferometric custom-built white-light spectroscopy setup capable of taking direct measurements of the transmittance and indirect measurements of the phase angle by means of Fourier-transform interferometry [62,63]. In order to reconstruct the amplitude and phase angle of the transmission coefficient as defined in the simulations, we performed reference measurements through the bare substrate of the metasurfaces.

By comparing the experimental results to predictions made with the same methodology as used in the design process but while considering slightly modified geometrical parameters, we identified the geometry that is most consistent with the measurements. A radius of $r = 251$ nm and a height of $h = 268$ nm for the nanocylinders has been identified. They slightly deviate from the ideal design parameters due to fabrication imperfections. The lattice constant was met precisely, as it can be controlled in the fabrication with very high precision.

With these parameters, adapted simulations of the transmission coefficients of all metasurfaces were performed by employing the local coordinate T-matrix method. For the numerical simulations we have used circa 441 particles with a multipole expansion up to the octupolar order. Figure 3 depicts a comparison of the numerical and experimental results. In Fig. 3(a), the numerical and experimental results show a very good agreement in the transmission coefficient for all types of metasurfaces. The square array metasurface is clearly in phase state *I*. With increasing disorder, i.e., the sequence: square array → perturbed square array → Matérn softcore → Matérn hardcore, the path of $t(\lambda)$ contracts and transitions into phase state *II* for the degree of disorder introduced by the

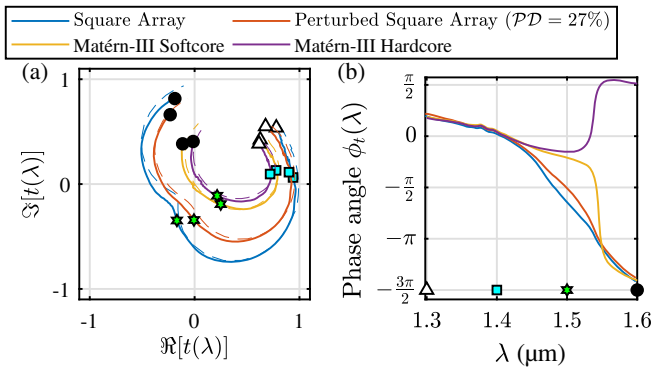

FIG. 3. Experimental measurement of (a) transmission coefficient $t(\lambda)$ and (b) its phase angle $\phi_t(\lambda)$ through four metasurfaces with different arrangements of equal density: Square array, perturbed square array, Matérn type-III soft-core and hard-core point processes, as shown in Fig. 2. Simulation results are shown with dashed lines of the same color.

Matérn type-III hardcore metasurface. Figure 3(b) emphasizes on the experimentally observed anomalous dispersion of the phase angle of the transmission coefficient for above-threshold disordered metasurfaces. In the SM Sec. V, we have included another set of experiments which demonstrates the transition from phase state *III* to phase state *II*.

In conclusion, we have reported a previously unknown feature of disordered dielectric metasurfaces: By increasing the disorder in the particle positions of a Huygens' metasurface above a critical threshold, the advance in the phase angle of the transmitted light can be switched from normal dispersion to anomalous dispersion. As the spectral detuning between the electric and magnetic dipole resonances increases, we have shown that the threshold in the positional disorder decreases for the transition from the normal to the anomalous dispersion phase state, and that it increases for the transition from the overlapping to the split resonances phase state. Finally, we performed full wave simulations of realistic structures and corroborated our findings with experiments. Our findings, from a fundamental point of view, are important in understanding complex light interaction in disordered media. We expect our insights to open yet another door for a variety of applications in the field of disordered photonics [11].

We acknowledge support by the German Research Foundation through the priority program SPP 1839 Tailored Disorder (PE 1524/10-1, STA 1426/1-1, and CR 3640/7-1). A. R. and R. N. S. also acknowledge support from the Karlsruhe School of Optics and Photonics (KSOP). D. A., S. F., M. F., T. P., and I. S. also acknowledge support by the Thuringian State Government within its ProExcellence initiative (ACP^{2020}). We acknowledge discussions with A. Mirlin and D. Dams on how to measure disorder.

A. R. and D. A. contributed equally to this work.

*aso.rahimzadegan@kit.edu
†dennis.arslan@uni-jena.de

[1] I. Staude and J. Schilling, Nat. Photonics **11**, 274 (2017).
[2] M. Decker, I. Staude, M. Falkner, J. Dominguez, D. N. Neshev, I. Brener, T. Pertsch, and Y. S. Kivshar, Adv. Opt. Mater. **3**, 813 (2015).
[3] A. I. Kuznetsov, A. E. Miroshnichenko, M. L. Brongersma, Y. S. Kivshar, and B. Luk'yanchuk, Science **354**, aag2472 (2016).
[4] I. Fernandez-Corbaton, Opt. Express **21**, 29885 (2013).
[5] S. Liu, A. Vaskin, S. Campione, O. Wolf, M. B. Sinclair, J. Reno, G. A. Keeler, I. Staude, and I. Brener, Nano Lett. **17**, 4297 (2017).
[6] S. Jahani and Z. Jacob, Nat. Nanotechnol. **11**, 23 (2016).
[7] M. I. Shalaev, J. Sun, A. Tsukernik, A. Pandey, K. Nikolskiy, and N. M. Litchinitser, Nano Lett. **15**, 6261 (2015).
[8] Y. F. Yu, A. Y. Zhu, R. Paniagua-Domínguez, Y. H. Fu, B. Luk'yanchuk, and A. I. Kuznetsov, Laser Photonics Rev. **9**, 412 (2015).
[9] K. E. Chong, L. Wang, I. Staude, A. R. James, J. Dominguez, S. Liu, G. S. Subramania, M. Decker, D. N. Neshev, I. Brener, and Y. S. Kivshar, ACS Photonics **3**, 514 (2016).
[10] K. E. Chong, I. Staude, A. James, J. Dominguez, S. Liu, S. Campione, G. S. Subramania, T. S. Luk, M. Decker, D. N. Neshev, I. Brener, and Y. S. Kivshar, Nano Lett. **15**, 5369 (2015).
[11] D. S. Wiersma, Nat. Photonics **7**, 188 (2013).
[12] M. Segev, Y. Silberberg, and D. N. Christodoulides, Nat. Photonics **7**, 197 (2013).
[13] I. M. Vellekoop, A. Lagendijk, and A. P. Mosk, Nat. Photonics **4**, 320 (2010).
[14] M. Albooyeh, S. Kruk, C. Menzel, C. Helgert, M. Kroll, A. Krysinski, M. Decker, D. N. Neshev, T. Pertsch, C. Etrich, C. Rockstuhl, S. A. Tretyakov, C. R. Simovski, and Y. S. Kivshar, Sci. Rep. **4**, 4484 (2014).
[15] M. Jang, Y. Horie, A. Shibukawa, J. Brake, Y. Liu, S. M. Kamali, A. Arbabi, H. Ruan, A. Faraon, and C. Yang, Nat. Photonics **12**, 84 (2018).
[16] P. Moitra, B. A. Slovick, Z. G. Yu, S. Krishnamurthy, and J. Valentine, Appl. Phys. Lett. **104**, 171102 (2014).
[17] W.-B. Shi, L.-Z. Liu, R. Peng, D.-H. Xu, K. Zhang, H. Jing, R.-H. Fan, X.-R. Huang, Q.-J. Wang, and M. Wang, Nano Lett. **18**, 1896 (2018).
[18] X. Shi, X. Chen, B. A. Malomed, N. C. Panoiu, and F. Ye, Phys. Rev. B **89**, 195428 (2014).
[19] A. V. Kolobov, P. Fons, A. I. Frenkel, A. L. Ankudinov, J. Tominaga, and T. Uruga, Nat. Mater. **3**, 703 (2004).
[20] A. Zylbersztejn and N. F. Mott, Phys. Rev. B **11**, 4383 (1975).
[21] M. Liu, H. Y. Hwang, H. Tao, A. C. Strikwerda, K. Fan, G. R. Keiser, A. J. Sternbach, K. G. West, S. Kittiwatanakul, J. Lu, S. A. Wolf, F. G. Omenetto, X. Zhang, K. A. Nelson, and R. D. Averitt, Nature (London) **487**, 345 (2012).
[22] Q. Wang, E. T. F. Rogers, B. Gholipour, C.-M. Wang, G. Yuan, J. Teng, and N. I. Zheludev, Nat. Photonics **10**, 60 (2016).
[23] B. Gholipour, J. Zhang, K. F. MacDonald, D. W. Hewak, and N. I. Zheludev, Adv. Mater. **25**, 3050 (2013).

[24] H. N. Krishnamoorthy, Z. Jacob, E. Narimanov, I. Kretzschmar, and V. M. Menon, in *Conference on Lasers and Electro-Optics* (OSA, San Jose, 2012), p. QM2E.6.

[25] I. I. Smolyaninov and E. E. Narimanov, Phys. Rev. Lett. **105**, 067402 (2010).

[26] M. V. Rybin, D. S. Filonov, K. B. Samusev, P. A. Belov, Y. S. Kivshar, and M. F. Limonov, Nat. Commun. **6**, 10102 (2015).

[27] A. Guo, G. J. Salamo, D. Duchesne, R. Morandotti, M. Volatier-Ravat, V. Aimez, G. A. Siviloglou, and D. N. Christodoulides, Phys. Rev. Lett. **103**, 093902 (2009).

[28] C. E. Rüter, K. G. Makris, R. El-Ganainy, D. N. Christodoulides, M. Segev, and D. Kip, Nat. Phys. **6**, 192 (2010).

[29] M. Verbin, O. Zilberberg, Y. E. Kraus, Y. Lahini, and Y. Silberberg, Phys. Rev. Lett. **110**, 076403 (2013).

[30] S. John, Phys. Rev. Lett. **58**, 2486 (1987).

[31] Y. Lahini, R. Pugatch, F. Pozzi, M. Sorel, R. Morandotti, N. Davidson, and Y. Silberberg, Phys. Rev. Lett. **103**, 013901 (2009).

[32] D. S. Wiersma, P. Bartolini, A. Lagendijk, and R. Righini, Nature (London) **390**, 671 (1997).

[33] J. Topolancik, B. Ilic, and F. Vollmer, Phys. Rev. Lett. **99**, 253901 (2007).

[34] M. Renner and G. von Freymann, Adv. Opt. Mater. **2**, 226 (2014).

[35] T. Baba, Nat. Photonics **2**, 465 (2008).

[36] E. Lidorikis, M. M. Sigalas, E. N. Economou, and C. M. Soukoulis, Phys. Rev. B **61**, 13458 (2000).

[37] C. Helgert, C. Rockstuhl, C. Etrich, C. Menzel, E.-B. Kley, A. Tünnermann, F. Lederer, and T. Pertsch, Phys. Rev. B **79**, 233107 (2009).

[38] C. Helgert, C. Rockstuhl, C. Etrich, E.-B. Kley, A. Tünnermann, F. Lederer, and T. Pertsch, Appl. Phys. A **103**, 591 (2011).

[39] T. Pertsch, U. Peschel, J. Kobelke, K. Schuster, H. Bartelt, S. Nolte, A. Tünnermann, and F. Lederer, Phys. Rev. Lett. **93**, 053901 (2004).

[40] See Supplemental Material at http://link.aps.org/supplemental/10.1103/PhysRevLett.122.015702 for a more detailed description of the analytic, numeric, statistical, and fabrication methods. This includes the Lorentz model used, the T-matrix formalism, the far-field transmission calculation, the phase diagram generation, the point process, statistical analysis, complementary experiments, and the fabrication procedure.

[41] R. A. DiStasio, G. Zhang, F. H. Stillinger, and S. Torquato, Phys. Rev. E **97**, 023311 (2018).

[42] E. C. Oğuz, J. E. S. Socolar, P. J. Steinhardt, and S. Torquato, Phys. Rev. B **95**, 054119 (2017).

[43] G. Zhang, F. H. Stillinger, and S. Torquato, Sci. Rep. **6**, 36963 (2016).

[44] S. Torquato and F. H. Stillinger, Rev. Mod. Phys. **82**, 2633 (2010).

[45] S. Torquato and F. H. Stillinger, Phys. Rev. E **68**, 041113 (2003).

[46] J. M. Ziman, *Models of Disorder: The Theoretical Physics of Homogeneously Disordered Systems* (Cambridge University Press, Cambridge, England, 1979).

[47] C. Kittel and H. Kroemer, *Thermal Physics* (Freeman, New York, 1980).

[48] J. Illian, A. Penttinen, H. Stoyan, and D. Stoyan, *Statistical Analysis and Modelling of Spatial Point Patterns* (Wiley, Chichester, 2008).

[49] J. E. Sipe and J. V. Kranendonk, Phys. Rev. A **9**, 1806 (1974).

[50] A. Rahimzadegan, R. Alaee, I. Fernandez-Corbaton, and C. Rockstuhl, Phys. Rev. B **95**, 035106 (2017).

[51] L. Novotny and B. Hecht, *Principles of Nano-Optics*, 2nd ed. (Cambridge University Press, Cambridge, England, 2012).

[52] M. Albooyeh, D. Morits, and S. A. Tretyakov, Phys. Rev. B **85**, 205110 (2012).

[53] I. Sersic, C. Tuambilangana, T. Kampfrath, and A. F. Koenderink, Phys. Rev. B **83**, 245102 (2011).

[54] J. D. Jackson and L. C. Levitt, *Classical Electrodynamics*, 3rd ed. (Wiley, New York, 1962).

[55] I. Fernandez-Corbaton and G. Molina-Terriza, Phys. Rev. B **88**, 085111 (2013).

[56] R. N. S. Suryadharma, M. Fruhnert, I. Fernandez-Corbaton, and C. Rockstuhl, Phys. Rev. B **96**, 045406 (2017).

[57] M. I. Mishchenko, L. D. Travis, and D. W. Mackowski, J. Quant. Spectrosc. Radiat. Transfer **55**, 535 (1996).

[58] R. Alaee, M. Albooyeh, and C. Rockstuhl, J. Phys. D **50**, 503002 (2017).

[59] I. Staude, A. E. Miroshnichenko, M. Decker, N. T. Fofang, S. Liu, E. Gonzales, J. Dominguez, T. S. Luk, D. N. Neshev, I. Brener, and Y. Kivshar, ACS Nano **7**, 7824 (2013).

[60] J. Møller, M. L. Huber, and R. L. Wolpert, Stoch. Proc. Appl. **120**, 2142 (2010).

[61] J. Teichmann, F. Ballani, and K. G. van den Boogaart, Spat. Stat. **3**, 33 (2013).

[62] E. Pshenay-Severin, F. Setzpfandt, C. Helgert, U. Hübner, C. Menzel, A. Chipouline, C. Rockstuhl, A. Tünnermann, F. Lederer, and T. Pertsch, J. Opt. Soc. Am. B **27**, 660 (2010).

[63] E. Pshenay-Severin, M. Falkner, C. Helgert, and T. Pertsch, Appl. Phys. Lett. **104**, 221906 (2014).